Future Journal of Pharmaceutical Sciences

RESEARCH Open Access

Antimicrobial and antioxidant therapy with bioactive plant molecules on Fe_3O_4 phytohybrid nanoplatforms

Janesline Fernandes, Teotone Vaz* and Tushar S. Anvekar

Abstract

Background: Nanobiomedicines have gained increasing attention for their potential to improve efficacy and are emerging as a promising therapeutic paradigm. Magnetic nanoconjugates loaded with bioactive drugs have the advantage of sustained circulation in the bloodstream and significantly reduced toxicity of therapeutic agents in a precise manner. The well-developed surface chemistry of Fe_3O_4 has led to the development better tools, promoting them as nanoplatforms with potential technological applications in biomedical sciences.

Results: Fe_3O_4 phytohybrids with Laxmitaru extract as the primary coating and loaded with Eugenol and Ylang-Ylang essential oils were successfully synthesized. The X-ray diffraction technique has revealed the high purity nanoparticle materials, as no additional impurity peaks were observed. Fourier transform infra-red spectra have confirmed the presence of a primary coating of Laxmitaru extract and a secondary layer of essential oil, as additional peaks and broadening are observed in drug-loaded Fe_3O_4 nanoparticles. Magnetic susceptibility values indicate the material's superparamagnetic nature. Transmission electron microscopy images have ensured that the particles were spherical, monodispersed, and in the range of 4.30 nm to 13.98 nm. Antimicrobial studies show inhibition zones on the microorganisms *S. Aureus* and *E. Coli* with enhanced activity. Drug entrapment efficiency studies revealed the encapsulation of drug molecules onto Fe_3O_4-Laxmitaru composite. Dynamic light scattering studies confirm the increase in hydrodynamic size, indicating the loading of essential oils and the decrease in polydispersity index ensures monodispersed nanoparticles. The antioxidant study showed the essential oils retained their antioxidant activity even after they were conjugated on Fe_3O_4-Lax composites.

Conclusions: Laxmitaru phytochemical-coated Fe_3O_4 nanoparticles were successfully conjugated with Eugenol and Ylang-Ylang essential oils. Our results provide a model therapeutic approach for the development of new alternative strategies for enhancing antimicrobial and antioxidant therapy, with potential advantages in the field of nanobiomedicine.

Keywords: Fe_3O_4 Nanoparticles, Nanoplatforms, Laxmitaru, Eugenol, Ylang-Ylang, Essential oils, Antimicrobial, Antioxidant therapy

Background

Nanoscience and nanotechnology are the most important research areas in modern science and allow researchers to produce important advances in healthcare science. Nanoscale drug delivery platforms have gained importance over the past few decades, which have shown promising clinical results in treating varieties of cancer and inflammatory disorders. This selective administration enhances therapeutic drug efficacy at targeted sites while minimizing the adverse side effects. The use of nanomaterials as carriers for drugs or other bioactive therapeutic agents has

*Correspondence: teovaz18@gmail.com
Department of Chemistry, St. Xavier's College, Mapusa, Goa, India

been widely investigated, with the focus to improve therapeutic effect, on-site release, and lowering of side effects of the administered drugs. Among magnetic materials, Fe_3O_4 nanoparticles (NPs) are extensively studied and are considered as promising drug carriers in nanomedicine, owing to their various advantages such as their unique size, excellent biocompatibility, strong affinity, extremely low toxicity, biodegradability, surface reactivity, superparamagnetic nature and other properties making them preferable from traditionally used materials [1–5]. Many regular treatment therapies have limitations in efficacy, which has led to the necessity of nanomedical innovations. A balanced perception of the relationship between inorganic nanomaterials and the biological system has led to the emergence of better solutions for individualized therapy regimes. The composite inorganic–organic NPs have significantly enhanced the identification, quantification of specific disease biomarkers, improving the clinical translation and utility of nanomaterials in the field of medicine [6, 7]. Several metals and metal oxide NPs have been investigated for biomedical use. ZnO NPs synthesized through eco-friendly and natural sources has shown promising results as antibacterial, antibiofilm and other biomedical applications [8].

Antimicrobial approach based on magnetic nanoparticles (MNPs)

Microbial infections are listed among the major health concerns, occurring globally, where in the recent past a variety of fungi, yeasts, and several other pathogenic microorganisms, are responsible for developing a drug resistance thereby enhancing frequency and occurrence of infections. Antimicrobial resistance (AMR) has led to high rates of mortality, economic losses, worsening of health care, increased diagnosis and treatment losses, thus giving rise to a need to develop new antibacterial agents and strategies against drug-resistant super-bugs [9]. One of the most enticing antimicrobial strategies is based on the use of MNPs to transport and control the release of active drugs at the diseased site. Due to the development of AMR to synthetic drugs, a strategy to use plant compounds having antimicrobial properties is being harnessed. MNPs being permeable to tissues and cells can be magnetically targeted to reach specific sites inside the body. This way the bioactive drugs can be delivered at the diseased site which conventional drugs may not reach by themselves. Additionally, this could also minimize undesirable side effects [10]. Due to targeted action, the toxic effects of drugs on healthy tissues can be avoided.

Fe_3O_4 conjugates as promising nanosystems

MNPs are attractive materials to develop novel routes for Targeted Drug Delivery (TDD) because of their well-developed surface chemistry, significant surface/area ratio, and superparamagnetism. Moreover, applications in biosystems require MNPs to be stable in water at pH 7 and in the physiological environment [10]. Fe_3O_4 NPs are preferred as it contains Fe^{+2} ions that have the potential to act as an electron donor. Though, they are magnetic materials, their residual magnetization is zero, a property observed to be beneficial to avoid coagulation which further lowers the in vivo agglomeration. Additionally, their high surface activity is vulnerable to oxidation in the air, affecting their magnetic and dispersibility property. Therefore, the functionalization of Fe_3O_4 NPs with hydrophilic and biocompatible polymers coating, prevents oxidation and provides colloidal stability, enhanced dispersibility, and ensures chemical binding/conjugation sites for drug molecules and other therapeutic agents to the superparamagnetic Fe_3O_4, thereby optimizing the biomedical utility for TDD [11–14].

The drug can be thus targeted to the desired site using an external magnetic field, avoiding delivery to healthy tissues. Fe_3O_4 NPs have been used with various synthetic and natural drugs to inhibit microbes that could cause serious infectious diseases. As they occur naturally in the human heart, spleen, and liver; they have been approved for clinical use by Food and Drug Administration (FDA) [3, 10]. Being nanosized, smaller concentrations of drug can be adsorbed on the particles and thus reducing the side effects and the exposure of the drug concentration at the infection site. The release of the drug can be controlled with respect to time of release and dosage [10, 15]. Bifunctional Fe_3O_4@Ag NPs prepared by reducing Ag ions on the surface of Fe_3O_4 NPs show both superparamagnetic and antibacterial properties [16]. Fatty acids assisted biologically synthesized superparamagnetic γ- Fe_2O_3 NPs ensure the stability to the NPs. They were investigated for antimicrobial, antibiofilm, and anti-cancer biomedical applications. Magnetic property was an advantage to boost the biological activity of γ- Fe_2O_3 NPs by the application of external magnetic field or in blend with other therapeutic drugs [17].

Simarouba glauca commonly known as Laxmitaru (Lax) plant was used as herbal medicine against dysentery. The crude bark and leaf water extracts contains active phytochemicals having several pharmacological properties such as antipyretic, hemostatic, anticancerous, antiparasitic, and anthelmintic besides antidysenteric properties [18]. Quassinoids are the major group of phytochemicals present and to date approximately 200 of them are isolated and structures elucidated [19]. In the present study, the concentrated water extract of Lax was

explored as the natural biocompatible organic coating on Fe_3O_4 NPs to stabilize the molecule. Thus making it immune friendly, being non-toxic with known medicinal benefits. Quassinoids present in the plant extract have antimalarial and cytotoxicity effects against several human cancer cell lines [18].

Eugenol (Eug) is an allyl chain-substituted guaiacol, i.e., 2-methoxy-4-(2-propenyl) phenol. It is a member of the allylbenzene class, colorless to pale yellow oily liquid extracted from certain essential oils especially from clove oil, nutmeg, cinnamon, and bay leaf. It is slightly soluble in water and soluble in organic solvents. Eug is used in perfumeries, flavorings, and in medicine as a local analgesic (topical), antiseptic, antifungal, and an anesthetic. Eug possesses significant antioxidant, anti-inflammatory, and cardiovascular properties [20].

Ylang-Ylang (Yla) is an essential oil from *Cananga Odorata,* a perfumed tree (medicinal) bearing yellow flowers. Extensively used by perfume, food industry, and aromatherapy for its powerful floral fragrance and flavor. It is water-insoluble and contains sesquiterpenes, monoterpenes, phenols, methyl benzoate, benzyl acetate, geranyl acetate, linalool, geraniol which contribute to its medicinal property. It has a vast spectrum of pharmacological activities such as antioxidant, antibiofilm, antimicrobial, antifungal, antiinflammatory, insect repellent, antidiabetic, antimalarial, antiseptic, additionally it has curative properties for internal infections of the colon, etc.[21].

The objectives of this investigation were to synthesize Lax-coated Fe_3O_4 phytochemical nanoparticles, load them with plant-derived bioactive drugs Eug and Yla, to characterize and confirm their structural morphology, the percentage of drug loading, evaluate antimicrobial and antioxidant activity. These characteristics contribute to the description as promising molecules in the development of a new strategy of drug delivery.

Methods

All materials used were of Analytical Reagent grade as procured without any further purification. Deionized and nitrogen-purged water was used to prepare all the solutions. Reagents used were $FeCl_3.6H_2O$ (99% pure), $FeSO_4.7H_2O$ (98.5% pure), NaOH (Laboratory Reagent), Eugenol (Laboratory Reagent) 98%, Ylang-Ylang 98% were used as commercially procured. Laxmitaru (dry leaves) were obtained from the local market.

Synthesis of Fe_3O_4 NPs

$FeCl_3.6H_2O$ and $FeSO_4.7H_2O$ were taken in the ratio of 2:1 and dissolved in acidified deionized water. Then 2 M NaOH was added dropwise, with constant stirring and the reaction temperature was maintained at 60 °C. The pH was maintained above 11. The black precipitate of Fe_3O_4 obtained was sonicated for 1 h, repeatedly washed with deionized water and ethanol, and finally separated and dried. The net reaction is: $2Fe^{+3} + Fe^{+2} + 4OH^- \rightarrow Fe_3O_4 + 4H^+$

In-situ synthesis of pristine Fe_3O_4 and Fe_3O_4—Lax-coated NPs

Lax solution was prepared by boiling Lax dry leaves in (approx. 100 mL) pure water for 1 h The content was filtered and used as Lax extract. To this, 2 M NaOH (100 mL) was added. Stoichiometrically prepared ferrite solution (100 mL) in the ratio of 1:2 ($FeSO_4.7H_2O$ and $FeCl_3.6H_2O$) was added dropwise to the Lax-extract. The suspension was incubated for 1 h at 90 °C with gentle stirring as reported elsewhere [22]. The reaction pH was maintained above 11 by adding 2 M NaOH solution. The Fe_3O_4-Lax colloidal suspension was washed with de-ionized water and then with ethanol. The phytohybrid-coated Fe_3O_4-Lax NPs were dried at 60 °C and then further treated for loading.

Biogenic synthesis of Fe_3O_4-Lax-Eug and Fe_3O_4-Lax-Yla nanoconjugates using essential oils

The Fe_3O_4-Lax NPs were then functionalized with bioactive plant-derived drugs Eug and Yla to prepare the double-layered Core/shell/secondary shell nanomaterials. Eug solution (20 mg/mL in ethanol) and Yla solution (1 mL/5 mL in ethanol) were prepared and added to a known quantity of Fe_3O_4-Lax NPs. The suspensions were stirred magnetically for several hours, allowed to settle overnight, separated and dried [14]. The drugs were attached to Fe_3O_4-Lax by adsorption.

Materials characterization

X-ray powder diffraction (XRD) was used to determine the crystal structure & particle size in the 2Θ range of 20°–80° (Philips PW 1840 XRD diffractometer). Fourier transformed infra-red (FTIR) (Thermo Nicolet iS5 spectrometer) spectra were recorded in the wave range of 4400 to 400 cm^{-1}. Magnetic measurements was studied using vibrating sample magnetometer (VSM) (Lake Shore Model 7404S) and saturation magnetization (Ms) values were calculated. The morphology of the nanoconjugate materials was analyzed by high-resolution transmission electron microscopy (HRTEM) (JOEL JEM 2100F instrument). The size distribution of the synthesized Fe_3O_4 NPs before and after surface modification was measured using dynamic light scattering (DLS) (Bechman Coulter Delsa Nano Analyzer) at scattering angle of 90° and 25 °C as discussed elsewhere [15]. The average diameters were calculated from the three individual measurements.

Bioactivity evaluation of Fe_3O_4—Lax phytohybrids loaded with Yla and Eug drug

Antimicrobial studies were carried out by the zone of inhibition (ZI) method using the borewell agar diffusion technique discussed elsewhere [15, 23–25]. This method was used to quantitatively determine the level of inhibition of the bacterial strains produced by the bioactive plant drugs Eug and Yla loaded on Fe_3O_4-Lax NPs. Antibacterial activity was tested against bacterial reference strains *Staphylococcus Aureus* (*S. Aureus*) (ATCC 6538) and *Escherichia Coli* (*E. Coli*). The nanoconjugates were individually dispersed in alkaline buffer and dimethylsulfoxide (DMSO) to obtain the test solutions of concentration 2 mg/mL and 40 µg/mL, respectively. Subsequently, wells were bored into Mueller Hinton agar plates, using a sterile 10-mm-diameter cork borer and aseptically dispensed with 100 µL of test solutions. The temperature and time duration of incubation was maintained at 37 °C for 24 h, respectively. The plates were monitored for ZI which were recorded in mm. For consistency, the experiment was performed in triplicate.

Drug entrapment efficiency (% EE) studies were carried out to for the quantitative estimation of the amount of drug Eug and Yla loading capacity of Fe_3O_4-Lax phytohybrids using a UV–Vis spectrophotometer (Thermo Scientific Evolution 201) in the range of 200 to 800 nm as reported elsewhere [11]. A solution of a known quantity of Eug and Yla was prepared in ethanol. To this, a known quantity of Fe_3O_4-Lax was added. The dispersion was stirred for 45 min, allowed to stand for 10 min, and then coated compounds were separated. Spectra of the solution which contained the unadsorbed Eug and Yla was recorded before and after the adsorption process.

In vitro free radical scavenging activity (RSA) was performed by the following the method given elsewhere [11, 26, 27]. In brief, the decolorization property of the stable DPPH (2,2 diphenyl-1-picrylhydrazyl) was used in presence of synthesized Fe_3O_4- phytohybrids. A measured quantity of synthesized Fe_3O_4 NPs was added to the known molarity of DPPH solution and incubated in dark for 15 min at room temperature. The intensity of purple color decreased significantly with time to yellow–brown and was measured using UV–Vis spectrophotometer (Thermo Scientific Evolution 201 model) at λ_{max} of 514 nm. The percentage RSA of Fe_3O_4 NPs- Lax and Eug was determined using the following expression.

RSA (%) = $[(Ac - As)/Ac] \times 100$, where *Ac* is the absorbance of the control DPPH at zero min; *As* is the absorbance in the presence of the Fe_3O_4 nanocomposite sample after 15 min.

Results

Structural morphology and particle size

X-ray powder diffraction (XRD) peaks were analyzed and indexed using Joint Committee on Powder Diffraction Standards files and compared with magnetite standards. Figure 1 shows the XRD pattern for all the Fe_3O_4 conjugates. Crystallite size measurements were determined from the full width at half maxima (FWHM) of the strongest reflection of (311) peak using the Debye–Sherrer approximation formula, which assumes the small crystallite size to be the cause of line broadening. The crystallite sizes calculated are given in Table 1.

Fourier transformed infra-red (FTIR) spectroscopy

FTIR was recorded in the % transmittance mode. Figure 2 shows the FTIR spectra of Fe_3O_4, Fe_3O_4-Lax, Fe_3O_4-Lax-Eug & Fe_3O_4-Lax-Yla. The absorption peak frequencies for all the peak intensities are shown in Table 2.

Magnetic measurements

Vibrating sample magnetometer (VSM) and saturation magnetization (Ms) values. Superparamagnetism plays a key role in targeting carriers in biomedical applications and the lack of hysteresis is one criterion to identify the product as superparamagnetic. The magnetic characterization was done at room temperature, with a magnetic field in the range of −15,000 Oe to+15,000 Oe. The parameters obtained from the hysteresis loops were Ms, remanence magnetization (Mr) and coercivity (Hc). Figure 3 shows the VSM spectra of Fe_3O_4, Fe_3O_4-Lax,

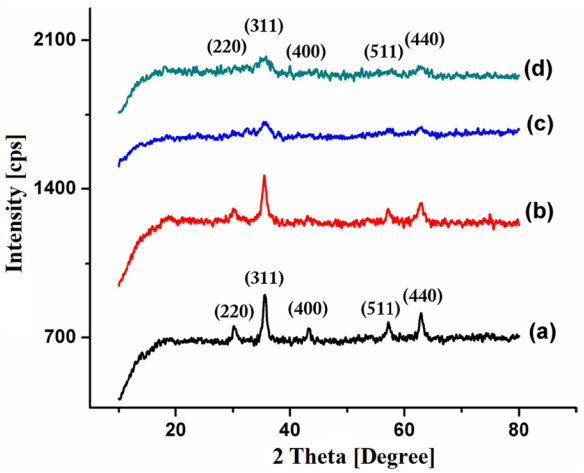

Fig. 1 XRD patterns of **a** Fe_3O_4, **b** Fe_3O_4-Lax, **c** Fe_3O_4-Lax-Eug, and **d** Fe_3O_4-Lax-Yla

Table 1 Particle size, Saturation magnetization (Ms) and Scavenging activity of phytohybrid Fe_3O_4 nanoconjugates

Phytohybrid conjugates	Particle size $D = \frac{k \times \lambda}{\beta \times \cos(\Theta)}$ nm (Debye–Scherrer formula)	Saturation magnetization (Ms) emu/g	% DPPH inhibition (scavenging activity)
(a) Fe_3O_4	22.35	51.40	No Activity
(b) Fe_3O_4-Lax	20.75	29.66	17
(c) Fe_3O_4-Lax-Eug	21.22	14.55	100
(d) Fe_3O_4-Lax-Yla	10.56	12.87	50

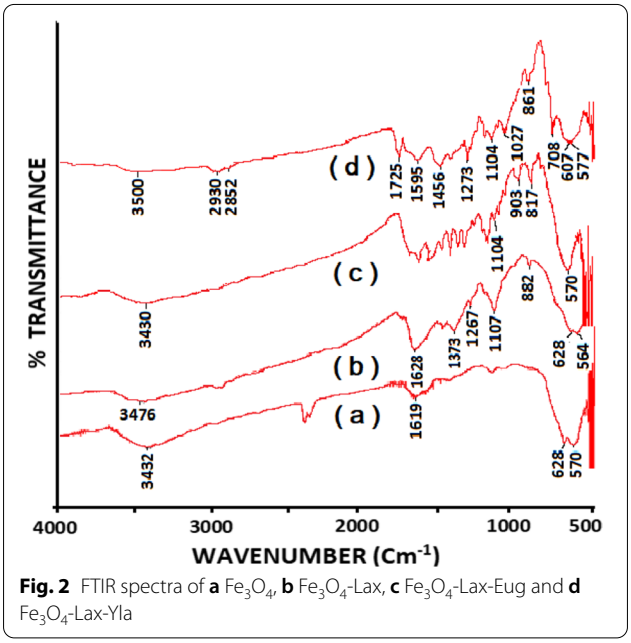

Fig. 2 FTIR spectra of **a** Fe_3O_4, **b** Fe_3O_4-Lax, **c** Fe_3O_4-Lax-Eug and **d** Fe_3O_4-Lax-Yla

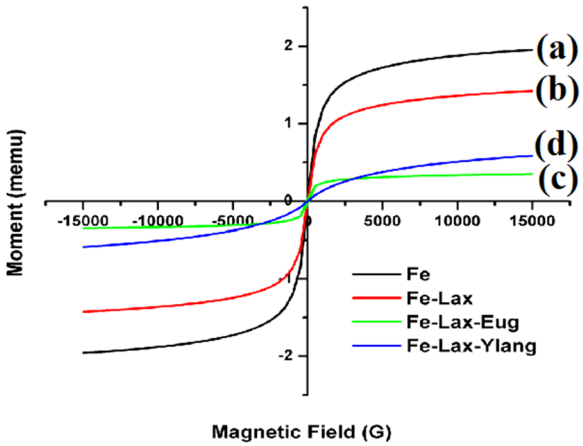

Fig. 3 VSM graphs of **a** Fe_3O_4, **b** Fe_3O_4-Lax, **c** Fe_3O_4-Lax-Eug and **d** Fe_3O_4-Lax-Yla

Fe_3O_4-Lax-Eug, Fe_3O_4-Lax-Yla. The Ms values are shown in Table 3.

High-resolution transmission electron microscopy (HRTEM)

Surface morphology and particle size. Figure 4 shows the HRTEM images of pure Fe_3O_4 NPs and coated conjugates. All the images illustrate that the average particle size was less than 20 nm. HRTEM analysis revealed that the mean core size of (a) Fe_3O_4 NPs was 4.30–12.78 nm, (b) Fe_3O_4-Lax was 4.44- 7.43 nm, (c) Fe_3O_4-Lax-Eug was 6.62–13.88 nm, and that of (d) Fe_3O_4-Lax-Yla was 7.64–13.98 nm, which is comparatively lesser than that of crystallite particle size calculated with XRD technique.

Antimicrobial activity

The functionalized magnetite materials proved a great antimicrobial effect, being active against both the Gram-positive pathogen *S. Aureus* and the Gram-negative pathogen *E. Coli.* The antimicrobial activity of the bio-active

Table 2 Assignments of the absorption bands in the FTIR spectra (cm^{-1})

Fe_3O_4 cm^{-1}	Fe-Lax cm^{-1}	Fe-Lax-Eug cm^{-1}	Fe-Lax-Yla cm^{-1}	Assignments
3435 –OH grps attached to core	3250	3400 broad	3400	V* H–O Stretching
-	2920	2941	2852, 2929	V*asy C-H of CH_2
1621-H–O-H of adsorbed water	1600, 1450, 1300	1637, 1593, 1421	1641, 1591, 1463, 1417	Delta *H-C–OH, C=O stretching
-	1290	-	-	Delta *H-C–OH
-	1150	1149, 1070, 1024	1188,1109, 1026	V*s C–O–C
-	870	916, 879, 844, 626	846, 786	C–C
600, 570	620, 560	615, 586	610, 598	Fe_{Td}-O–Fe_{Oh} & Fe_{Td}-Fe_{Oh}

Table 3 Zone of inhibition for (a) references/controls and (b) Fe_3O_4-Lax nanoconjugates

Sample	Zone of Inhibition (mm) *E. Coli*	Zone of Inhibition (mm) *S. Aureus*
(a)		
(a) Fe_3O_4	0	0
Lax	10	11
Eug	15	14
Yla	0	11
(b)		
(b) Fe_3O_4-Lax	14	
(c) Fe_3O_4-Lax-Eug	23	23
(d) Fe_3O_4-Lax-Yla	29	12

plant drugs loaded on Fe_3O_4-Lax phytohybrids was studied using common *E. Coli* and *S. Aureus.* The ZI data obtained have been summarized in Table 3.

Dynamic light scattering (DLS) studies

Particle size study was carried out using intensity distribution by DLS technique. Size distribution of Fe_3O_4 before and after surface modification was investigated in water at 25 °C. The size distribution and stability of the drug-loaded Fe_3O_4 NPs suspension was observed and recorded in Fig. 5.

Drug entrapment efficiency (% EE)

Drug entrapment efficiency (% EE) were analyzed using absorbance of the solution which contained the unadsorbed Eug and Yla was recorded before and after the adsorption process. The % EE values calculated, the values are given in Table 5 and the UV–Vis spectra are shown in Fig. 6.

In vitro free radical scavenging activity

Figure 7 illustrates spectra of antioxidant activity by Fe_3O_4-Lax-loaded Eug and Yla phytohybrids. DPPH inhibition values (%) on the Fe_3O_4 nanoconjugates are given in Table 1.

Discussion

The focus of this investigation was to synthesize pure Fe_3O_4 NPs with Lax coating and create nanoplatforms, loaded with bioactive drug molecules of Eug and Yla. Obtaining pure conjugates in nanosize was essential, which was confirmed by studying structural morphology and particle size. Figure 1 shows X-ray powder diffraction patterns of the prepared phytohybrid nanoconjugates. The XRD pattern of Fe_3O_4 NPs could be clearly indexed with JCPDS File No. 65-3107. The lattice constant *a* was found to be 8.11A° and the diffraction peaks indexed as planes with d_{hkl} (220), (311), (400), (422), (511) and (440) stand for cubic unit cell, characteristic and confirming the formation of cubic inverse spinel crystal system of the Fe_3O_4 structure, with the strongest reflection at (311). The absence of any characteristic peak for impurities confirmed that all the materials were pure. No shift in the peak positions in all the XRD patterns was observed, which confirms that the binding process did not result in the phase change of the magnetic Fe_3O_4 NPs [28]. The size falls in the nanometer range, confirming the formation of nanosized Fe_3O_4 NPs. Table 1 illustrates the crystallite particle size gradually decreases from 22.85 to 10.56 nm with the loading of Lax as stabilizing layer on Fe_3O_4 and further with Eug and Yla. It is also observed that in the coated Fe_3O_4 nanocomposites, the peak intensities were weakened and peak width was broadened which confirms the attachment of the coating agent on the Fe_3O_4. In drug-loaded Fe_3O_4, the peak intensity further decreases, which is attributed to the fact that the coating and drug molecules are organic in nature, giving amorphous nature to the XRD patterns, which confirms the presence of coatings. Broad diffraction peaks in the XRD pattern of coated Fe_3O_4 also indicate a further decrease in particle size after coating due to reduced agglomeration and particles tend to monodisperse.

FTIR spectra in Fig. 2 have provided structural insight into the nanoconjugates and confirm the loading of biomolecules on Fe_3O_4 NPs. The characteristic absorption peaks at 628 and 576 cm^{-1} confirm the formation of Fe_3O_4 NPs and coated Fe_3O_4 conjugates in agreement with the literature [22]. Additional peaks and broadening are observed in drug-loaded Fe_3O_4, confirming the presence of Lax, Eug, or Yla. The weak intensity of the absorption peaks indicates the interactions between the Fe_3O_4 NPs and the coating substances are of an intermolecular type.

The H–O–H bending vibration peaks of H_2O seen in the range of 1000–1600 cm^{-1} have a weak intensity. The Fe_3O_4 materials exhibit two characteristic peaks in the range 690 to 550 cm^{-1}, assigned to Fe–O bonding in the Fe_3O_4 crystal lattice and represent the stretching vibrations bands, related to the Fe metal in the octahedral and tetrahedral sites, respectively, in the spinel oxide structure. The peak observed at 3432 cm^{-1} for Fe_3O_4 material relates to –OH groups and H_2O groups on the surface of Fe_3O_4 NPs, which was shifted to 3450 cm^{-1}, and 3500 cm^{-1} in the coated samples of Fe-Lax, and Lax-Yla/Eug, respectively. The shift indicates the interaction between Lax, Eug, and Yla on the bare Fe_3O_4, in agreement with the literature [29, 30]. The peaks at 2930 c m^{-1} and 2852 cm^{-1} observed show the C–H stretching vibration. Some new peaks appear in the coated

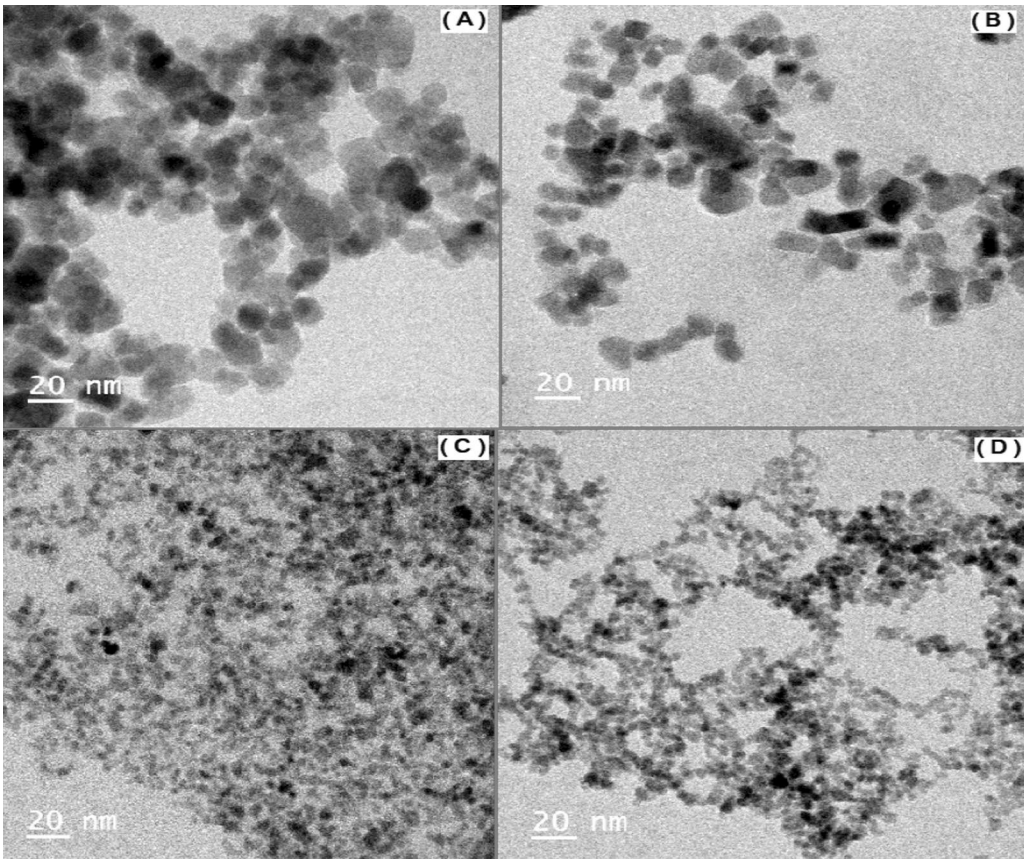

Fig. 4 HRTEM graphs of **A** Fe_3O_4 NPs, **B** Fe_3O_4-Lax, **C** Fe_3O_4-Lax-Eug and **D** Fe_3O_4-Lax-Yla

Fe_3O_4 and broadening of some peaks, indicate the intermolecular bonding between Lax and Fe_3O_4. When Fe_3O_4-Lax was coated with Eug & Yla, assignments are shifted for all the peaks. A shift in the Fe–O band is also observed. Thus, it could be confirmed that Lax, Eug, and Yla were attached to the Fe_3O_4 successfully. No impurity peaks were observed in any of the spectra, showing all the compounds formed were pure. The spectra were matched with standard literature data [29, 30].

Figure 3 shows the VSM spectra and the extracted parameters values of Ms, Mr and Hc are shown in Table 3. The absence of a hysteresis loop in all the graphs confirms the prepared nanoconjugates are superparamagnetic. Such materials have high Ms and zero coercivity and remanence magnetization. The magnetic moment of the particles, in the presence of magnetic field H, will align with the magnetic field direction, leading to a macroscopic magnetization of the compounds. The magnetization approached saturation when the magnetic field was increased to 15,000 Oe. The Ms values depend on the synthesis method and particle size. The Ms value of Fe_3O_4 NPs is high and matches well with standard magnetite values. The Ms values of coated Fe_3O_4 decrease, confirming the presence of coatings on the Fe_3O_4. On coating of the Fe_3O_4 NPs, the particle size decreases and thus Ms value decreases, which is attributed to the incorporation of Fe_3O_4 MNPs into Lax-Eug and Lax-Yla systems, which added a thick polymer layer on the particle surface [28]. Decreased Ms values also confirms that the particles behave as single domains. However, this amount of Ms is sufficient for biological applications of the ferrofluids in their use as drug carriers, under the application of an external magnetic field.

TEM analysis revealed that the mean core size of Fe_3O_4 NPs was 4.30–17.48 nm, Fe_3O_4-Lax was 4.44–15.43 nm, Fe_3O_4-Lax-Eug was 6.62–13.88 nm and that of Fe_3O_4-Lax-Yla was 7.64–13.98 nm, which are comparatively lesser than that of crystallite particle size calculated with XRD technique. As expected, the TEM size is smaller for the conjugate nanomaterials. Such small sizes are of great help to the superparamagnetic Fe_3O_4 drug-loaded NPs which enables the passive tissue targeting due to enhanced permeability, sustained release, and retention capacity upon administration. In addition, it is also

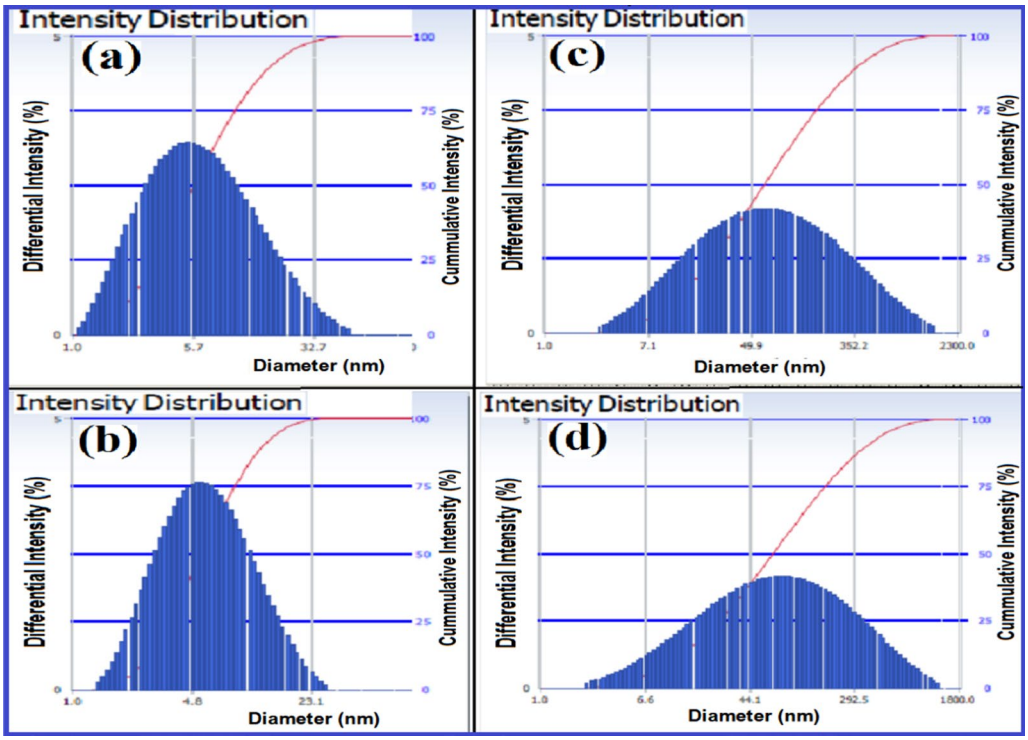

Fig. 5 Size distribution analysis of drug loaded Fe_3O_4 NPs by DLS

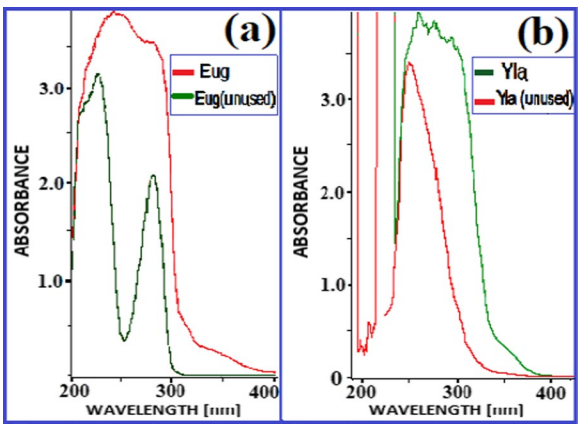

Fig. 6 UV–Vis spectra of **a** Eug and **b** Yla pure and on Fe-Lax adsorption

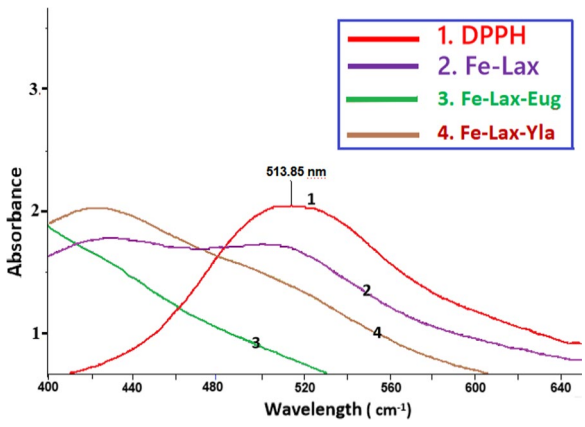

Fig. 7 Spectra of antioxidant activity by Fe_3O_4-Lax loaded Eug and Yla phytohybrids

possible to obtain the desired fine-tune ratio of hydrophilic and hydrophobic nature of conjugates, besides the whole molecular weight to manipulate the particle size and optimize the delivery efficiency [31]. The degree of agglomeration decreased after coating with Lax, Eug, and Yla, showing spherical-shaped monodispersed particles. The images show the amorphous nature of particles due to the presence of organic coatings on them.

Antimicrobial tests by the zone of inhibition (ZI) method as crucial studies were carried out to quantitatively determine the level of inhibition of the bacteria by the nanoconjugates explains the efficacy of the drug molecules under investigation. The bacteria under study were commonly found *E. coli* and *S. aureus.* It is seen in Table 3a that the ZI for Eug & Yla is 15 mm and zero, respectively, revealing that by themselves they have

Table 4 Cummulant particle size D(h) and polydispersity index (PI)

Phytohybrid conjugates	Cummulant Results Particle size D(h) (nm)	Polydispersity Index (PI)
a) Fe_3O_4	22.1	1.409
b) Fe_3O_4-Lax	18.3	0.368
c) Fe_3O_4-Lax-Eug	65.4	0.930
d) Fe_3O_4-Lax-Yla	72.0	0.468

less or no activity against the bacteria *E. Coli*. The values of ZI for coated Fe_3O_4 are represented in Table 3b. It was observed that there is a synergistic increase in the antibacterial activity of the drugs Eug & Yla when loaded on Fe_3O_4-Lax. The ZI values confirm the bactericidal activity, and it is assumed that the drug-coated Fe_3O_4 are stable in the bio medium which further stabilizes the drug-loaded onto them. Therefore, the retention time between the stable coated Fe_3O_4 and the bacterium increases, which then modulates the bacterial proteins and thus arrest bacterial growth in agreement with the literature [2]. The nanoconjugates under study have shown noteworthy antimicrobial activities against gram-negative bacteria *E. Coli* in comparison to gram-positive *S. Aureus,* although the mode of action and mechanism of their antimicrobial activities have not been clarified. The stronger interactions of Eug and Yla loaded on Fe_3O_4—Lax phytohybrids on the thinner cell wall of Gram-negative bacteria of *E. Coli* due to the surface charge and surface energy may be responsible for the better antimicrobial activity. Thus, it was concluded that by using the combination of biocompatible coated Fe_3O_4 along with the plant-derived drugs, there was enhanced antimicrobial activity. The study says that the dosage of the drug required for any illness can be decreased by this method as the drug is entirely released at the site of infection by using an external magnetic field [10]. This proves that drug-loaded-Fe_3O_4 NPs greatly enhances the activity of the drug and can act as good drug carriers.

The amount of drug Eug and Yla loaded on Fe_3O_4 NPs was measured as drug entrapment efficiency (% EE) in the range of 200 to 800 nm. After the adsorption process, the absorption peak intensity of Eug /Yla decreases indicating that some amount of the drug is adsorbed on the Fe_3O_4-Lax conjugates. As seen in Fig. 6, the UV–Vis spectra, there was good adsorption of all the drugs on Fe_3O_4-Lax. This indicates that the drugs were encapsulated onto Fe-Lax conjugates, with relatively high % EE values which is due to strong hydrophobic interaction between the plant drugs and the Fe-Lax conjugates. Therefore these Fe_3O_4 could act as drug carriers.

The significant increase in hydrodynamic size D(*h*) can be associated with the core–shell expansion after loading Fe_3O_4 with Lax, Eug, and Yla. As seen in Table 4, polydispersity index (PI) values decrease indicating high dispersion of the nanoparticles after loading with Lax extract and the drugs. The hydrodynamic size and PI values exhibit stability of Fe_3O_4 NPs in blood circulation time [16] (Table 5).

Conclusions

In conclusion, the plant-derived drug-loaded functional Fe_3O_4 NPs as a base were explored for enhanced antibacterial and antioxidant therapy, with potential advantages in the field of nanobiomedicine. Successfully synthesized Fe_3O_4 nanoconjugate materials viz. Fe_3O_4, Fe_3O_4-Lax, Fe_3O_4-Lax-Eug & Fe_3O_4-Lax-Yla were characterized for nanorange of 4.30 to 13.98 nm, spherical, monodispersed, high purity, the presence of coatings and secondary shell drug coatings and for the material's superparamagnetic nature. The antimicrobial activity show inhibition zones on the microorganisms with enhanced activity. These nanoconjugates proved to be efficient for stabilizing and controlling the release of the drugs. The results affirm that the phytohybrid derived Fe_3O_4-Lax-Eug & Fe_3O_4-Lax-Yla nanoconjugates are prototype alternatives in the exploring of new strategies to eradicate and prevent microbial infection that entail resistance.

Table 5 EE (%) value for Eug and Yla on Fe_3O_4- Lax phytohybrids

Sample	λ_{max} of Eug/Yla (nm)	Intensity before the drug absorption	Intensity after the drug absorption	Entrapment efficiency (%)	Recovered drug (%)
Fe_3O_4- Lax-Eug	428.65	0.603	0.440	27.18	72.96
Fe_3O_4-Lax-Yla	207.61	1.063	0.737	31.25	69.33

Abbreviations
Fe_3O_4: Iron oxide; NPs: Nanoparticles; MNPs: Magnetic nanoparticles; AMR: Antimicrobial resistance; Lax: Laxmitaru; Eug: Eugenol; Yla: Ylang-Ylang; RSA: Radical scavenging activity; Td: Tetrahedral; Oh: Octahedral; XRD: X-ray powder diffraction; FWHM: Full width at half maxima; FTIR: Fourier transformed infrared; Ms: Saturation magnetization; DPPH: (2,2 Diphenyl-1-picrylhydrazyl); *Ac*: Absorbance of the control DPPH at zero min; *As*: Absorbance in the presence of the Fe_3O_4 nanoconjugate; Mr: Remanence magnetization; Hc: Coercivity; VSM: Vibrating sample magnetometer; HRTEM: High-resolution transmission electron microscopy; ZI: Zone of inhibition; *E. coli*: *Escherichia coli*; *S. aureus*: *Staphylococcus aureus*; DLS: Dynamic light scattering; PI: Polydispersity index; % EE: Percentage entrapment efficiency; UV–Vis: Ultra violet–visible; D(*h*): Hydrodynamic size.

Acknowledgements
Ms. Fami Fernandes, Jesvita Cardozo and Ms. Kanica Shetye for assisting in experimental work. Department of Microbiology and Biotechnology, St. Xavier's College, Goa; SAIF- IIT, Madras; SAIF-IIT, Mumbai; National Institute of Oceanography (for XRD analysis), Dona Paula, Goa and BITS Pilani—Goa centre (for DLS study)

Authors' contributions
JF: Literature search, experimental work, results verification, rough and revision of draft and approval of manuscript. TV: Literature search, experimental work, draft revision, approval and communication of manuscript. TSA: Research Supervisor, conceptualization of proposed work, lead the discussions, authenticity of results, interpretation of results, final revision and approval of manuscript. All authors have read and approved the final manuscript.

Authors' information
JF: Research Scholar and Associate Professor, gaining expertize in synthesis of nanosystems for targeted drug delivery etc., Presented research papers at State, National and International levels. Awarded 1st Place for Oral paper presentation at ISCA Conference, Pune in December 2018.
TV: Senior Ph. D. and Associate Professor, Research collaborator in the team, published 06 articles. Area of Specialization: Inorganic synthesis, Nanomaterials, Characterization, Catalysis, Solid-State, Targeted drug delivery Photodegradation, etc.
TSA: Professor in Chemistry, Ph. D. Guide and Team leader, 04 Ph. D. students, Area of Specialization: Inorganic synthesis, Nanomaterials, Characterization, Catalysis, Solid-State, Photodegradation, Pharmaceutical synthesis, 15+ Research article, 02 Book Chapters, etc.

Funding
Not applicable.

Availability of data and materials
All data generated or analyzed during this study are included in this published article.

Declarations

Ethics approval and consent to participate
Not applicable.

Consent for publication
Not applicable.

Competing interests
The authors declare that they have no competing interests.

Received: 21 April 2021 Accepted: 11 October 2021
Published online: 24 October 2021

References

1. Shen L, Li B, Qiao Y (2018) Fe_3O_4 nanoparticles in targeted drug/gene delivery systems. Materials 11:324. https://doi.org/10.3390/ma11020324
2. Dorniani D, Kura AU, Hussein-Al-Ali SH, Hussein MZB, Fakurazi S, Shaari AH, Ahmad Z (2014) In-vitro sustained release study of Gallic acid coated with Magnetite-PEG and Magnetite-PVA for drug delivery system. Sci World J 2–3:416354. https://doi.org/10.1155/2014/416354
3. Xie J, Lee S, Chen X (2010) Nanoparticle-based theranostic agents. Adv Drug Delivery Rev 62(11):1064–1079. https://doi.org/10.1016/j.addr.2010.07.009
4. Mandal TK, Patait V (2021) Utilization of nanomaterials in target oriented drug delivery vehicles. J Sci Res 13(1):299–316. https://doi.org/10.3329/jsr.v13i1.47690
5. Nikezić AVV, Bondžić AM, Vasić VM (2020) Drug delivery systems based on nanoparticles and related nanostuctures. Eur J Pharm Sci 1(151):105412. https://doi.org/10.1016/j.ejps.2020.105412
6. Adeola HA, Sabiu S, Adekiya TA, Aruleba RT, Aruwa CE, Oyinloye BE (2020) Prospects of nanodentistry for the diagnosis and treatment of maxillofacial pathologies and cancers. Heliyon 6(9):e04890. https://doi.org/10.1016/j.heliyon.2020.e04890
7. Akbarzadeh A, Samiel M, Davaran S (2012) Magnetic nanoparticles: preparation, physical properties and applications in biomedicine. Nanoscale Res Lett 7:144. https://doi.org/10.1186/1556276X-7-144
8. Ali SG, Ansari MA, Jamal QMS, Almatroudi A, Alzohairy MA, Alomary MN, Rehman S, Mahadevamurthy M, Jala M, Khan HM, Adil SF, Khan M, Al-Warthan A (2021) Butea monosperma seed extract mediated biosynthesis of ZnO NPs and their antibacterial, antibiofilm and anti-quorum sensing potentialities. Arabian J Chem 14(4):103044. https://doi.org/10.1016/J.Arabjc.2021.103044
9. Teixera MC, Carbone C, Sousa MC, Espina M, Garcia ML, Lopez ES, Souto EB (2020) Nanomedicines for the delivery of antomicrobial peptides. Nanomaterials 10:560. https://doi.org/10.3390/nano10030560
10. Liakos I, Mihai A, Holban AM (2014) Magnetic nanostructures for antiinfectious therapy. Molecule 19(8):12710–12726. https://doi.org/10.3390/molecules190812710
11. Khalkhali M, Sadighian S, Rostamizadeh K, Khoeini F, Naghibi M, Bayat N, Habibizadeh M, Parsa M, Hamidi M (2015) Synthesis and Characterization of Dextran coated magnetite nanoparticles for simultaneous Diagnostics and Theraphy. BioImpacts DARU J Pharm Sci 23:45. https://doi.org/10.15171/bi.2.19
12. Rasouli E, Basirun WJ, Rezayi M, Shameli K, Nourmohammadi E, Khandanlou R, Izadiyan Z, Sarkarizi HK (2018) Ultrasmall superparamagnetic Fe_3O_4 nanoparticles: honey-based green and facile synthesis and in vitro viability assay. Int J Nanomed 13:6903–6911. https://doi.org/10.2147/IJN.S158083
13. Liao N, Wu M, Pan F, Lin J, Li Z, Zhang D, Wang Y, Zheng Y, Peng J, Liu X, Liu J (2016) Poly (dopamine) coated superparamagnetic Iron oxide nanocluster for non invasive labeling, tracking, and targeted delivery of adipose tissue-derived stem cells. Sci Rep 6:18746. https://doi.org/10.1038/Srep18746
14. Yin H, Zhang H, Liu B (2013) Superior anticancer efficacy of curcumin loaded nanoparticles against lung cancer. Acta Biochim Biophys Sin 45(8):634–640. https://doi.org/10.1093/abbs/gmt063
15. Grumezescu AM, Gestal MC, Holban AM, Grumezescu V, Vasile BS, Mogoanta L, Iordache F, Bleotu C, Mogosanu GD (2014) Biocompatible Fe_3O_4 increases the efficacy of amoxicillin delivery against Gram-Positive and Gram-Negative Bacteria. Molecules 19(4):5013–5027. https://doi.org/10.3390/molecules19045013
16. Gong P, Li H, He X, Wang K, HU j, Tan W, Zhang S, Yang X, (2007) Preparation and antibacterial activity of Fe_3O_4 @ Ag nanoparticles. Nanotechnology 18:255604. https://doi.org/10.1088/0957-4484/18/28/285604
17. Ansari MA, Asiri SMM (2021) Green synthesis, antimicrobial, antibiofilm and antitumor activities of superparamagnetic γ-Fe_2O_3 NPs and their molecular docking study with cell wall mannoproteins and peptidoglycan. Int J Biol Macromol 171(28):44–58. https://doi.org/10.1016/J.Ijbiomac.2020.12.162
18. Patil MS, Gaikwad DK (2011) A critical review on medicinally important oil yielding plant Laxmitaru (Simarouba glauca DC). J Pharm Sci Res 3(4):1195–1213
19. Jose A, Kannan E, Kumar PRAV, Madhunapantula SRV (2019) Therapeutic potential of phytochemicals isolated from *Simarouba glauca* for inhibiting cancers: a REVIEW. Sys Rev Pharm 10(1):73–80. https://doi.org/10.5530/srp.2019.1.12

20. Heghes SC, Vostinaru O, Rus LM, Mogosan C, Iuga CA, Filip L (2019) Antispasmodic effect of essential oils and their constituents: a review. Molecules 24:1675. https://doi.org/10.3390/molecules24091675
21. Bilcu M, Grumezescu AM, Oprea AE, Popescu RC, Mogosanu GD, Hristu R, Stanciu GA, Mihailescu DF, Lazar V, Bezirtzoglou E, Chifiriue MC (2014) Efficiency of Vanilla, Patchouli and Ylang Ylang essential oils stabilized by Iron Oxide @ C_{14} nanostructures against bacterial adherence and biofilms formed by *Staphylococcus aureus* and *Klebsiella pneumoniae* clinical strains. Molecules 19:17943–17956. https://doi.org/10.3390/molecules191117943
22. Ciobanu CS, Andronescu E, Pall L (2010) Physico-chemical properties of iron oxide-dextrin thin films. Rev Chim Bucharest 61(12):231589982
23. de Carvalho JF, de Azevedo IM, Rocha KBF, Medeiros AC, Carriço AS (2017) Oxacillin magnetically targeted for the treatment of Methicillin-Resistant *S. aureus* infection in rats. Carriço Acta Cir Bras 32(1):46–55. https://doi.org/10.1590/s0102-865020170106
24. Iconaru SL, Prodan AM, Heino MM, Sizaret S, Predoi D (2012) Synthesis and characterization of polysaccharide - maghemite composite nanoparticles and their antibacterial properties. Nanoscale Res Lett 7:576. https://doi.org/10.1186/1556-276x-7-576
25. Raut P, Dhawale S, Kulkarni D, Pekamwar S, Shelke S, Panzade P, Paliwal A (2021) Pharmacodynamic findings for the usefulness of *Luffa cylindrica* (L.) leaves in atherosclerosis therapy with supporting antioxidant potential. Future J Pharm Sci 7:38. https://doi.org/10.1186/s43094-021-00185-8
26. Sajeeda N, Kolgi RR, Shivakumara SL, Shivaraj Y, Karigar CS (2019) Comparative phytochemical profile and antioxidant property of bark, flowers and leaves extracts of *simarouba glauca*. Asian J Pharm Clin Res 12(9):56–63. https://doi.org/10.22159/ajpcr.2019.v12i9.34211
27. Kadu S, Attarde D, Kulkarni D, Shelke S, Arsul V (2021) Comparative evaluation of multiple extracts of pericarp of *Luffa acutangula* (L.) for its significant antioxidant, antibacterial and antifungal activity. Res J Pharm Technol 14(4):1847–1853. https://doi.org/10.52711/0974-360x.2021.00327
28. Hussein-Al-Ali SH, Zowalaty ME, Kura AU (2014) Antimicrobial and controlled release studies of novel nystatin conjugated iron oxide nanocomposites. Biomed Res Int. https://doi.org/10.1155/2014/651831
29. Wembabazi E, Mugisha PJ, Ratibu A, Wendiro D, Kyambadde J, Vuzi PC (2015) Spectroscopic analysis of heterogeneous biocatalysts for biodiesel production from expired sunflower cooking oil. J Spectrosc. https://doi.org/10.1155/2015/714396
30. Tambe E, Gotmare S (2020) FTIR & GC-MS analysis of Ylang Ylang oil, comparative study of its chemical composition and concern regarding Diethyl phthalate. Res J Sci Eng Technol 10(2):35–47
31. Cao Y, Gao M, Chen C, Fan A, Zhang J, Kong D, Wang Z, Peer D, Zhao Y (2015) Triggered release polymeric conjugate micelles for on-demand intracellular drug delivery. Nanotechnology 26:115101. https://doi.org/10.1088/0957-4484/26/11/115101

Publisher's Note